Elastic behaviour of a wedge disclination dipole near a sharp crack emanating from a semi-elliptical blunt crack*

Song Hao-Peng(宋豪鹏), Fang Qi-Hong(方棋洪), and Liu You-Wen (刘又文)†

College of Mechanics and Aerospace, Hunan University, Changsha 410082, *China*

(Received 18 January 2009; revised manuscript received 4 December 2009)

The interaction between a wedge disclination dipole and a crack emanating from a semi-elliptic hole is investigated. Utilising the complex variable method, the closed form solutions are derived for complex potentials and stress fields. The stress intensity factor at the tip of the crack and the image force acting on the disclination dipole center are also calculated. The influence of the morphology of the blunt crack and the position of the disclination dipole on the shielding effect to the crack and the image force is examined in detail. The results indicate that the shielding or anti-shielding effect to the stress intensity factor increases when the wedge disclination dipole approaches the tip of the crack. The effects of the morphology of the blunt crack on the stress intensity factor of the crack and the image force are very significant.

Keywords: wedge disclination dipole, blunt crack, shielding effect, image force

PACC: 6170G, 6220M, 4630N

1. Introduction

Disclinations are very important lattice defects with a long range distortion field analogous to dislocations. A unit disclination is a special and very strong source of internal elastic stress and possesses an energy which is very large in comparison with the energy of a dislocation. However in the case of self-screened disclination configurations, such as disclination dipoles and disclination loops, the energy may be relatively small and disclinations can exist in crystalline and amorphous materials.[1] Disclination elastic fields determine many of the physical properties of the phenomena in the deformation process of materials. As a result, a great deal of work was conducted on the elastic fields and elastic energies produced by screened disclinations.[1−5]

On the other hand, dislocations/disclinations in the vicinity of a crack tip play an important role in fracture mechanics. When plastic deformation has occurred around a crack tip, the stress field in the vicinity of the tip alters. One of the mechanisms, the dislocation emitted from the crack tip into the plastic zone, can reduce the stress intensity factor at the crack tip. This phenomenon is known as the dislocation/disclination shielding effect.[6] Apart from the dislocation/disclination shielding effect, the crack blunting is another important mechanism which can reduce the stress field around the crack tip. Hence, the interaction between dislocations/disclinations and blunt cracks has prompted many investigations.[7−9] Vehoff and Neumann[10] provided experimental evidence that the crack widens as it propagates, but its tip still remains sharp. In addition, Ohr[11] also provided experimental evidence that the emission of a dislocation from crack tip results in crack blunting. When the crack is blunted to a certain extent, the emission of dislocations from a crack tip can be interrupted. The blunted crack will not propagate until the nucleation of a new sharp crack. The dislocation may be re-emitted from a sharp crack emanating from the blunt crack. Shiue and Lee[12] considered the problem of the elastic interaction between screw dislocations and the blunt crack with a sharp crack. In addition, indentations at the surface of materials often bring about cracks and finally lead to fracture. Therefore the elastic interaction between a screw dislocation dipole and a sharp crack emanating from a surface semi-elliptic hole was investigated by Yang *et al.*[13] However, the problem of a wedge disclination dipole interacting with a crack emanating from a surface semi-elliptic hole has not been studied due to the complexity of the calculation. Hence, the purpose of this work is to discuss the effect of the morphology of

*Project supported by the National Natural Science Foundation of China (Grant Nos. 10872065 and 50801025), the Natural Science Foundation of Hunan Province of China (Grant No. 09JJ4003) and the Hunan Provincial Innovation Foundation for Postgraduate, China (Grant No. CX2009B067).

†Corresponding author. E-mail: liuyouw8294@sina.com

© 2010 Chinese Physical Society and IOP Publishing Ltd

the blunt crack and the position of the wedge disclination dipole on the shielding effect and the image force, which can give a better insight into plastic deformation mechanism and fracture and a better understanding of the mechanisms of strengthening and toughening of materials.

In the present paper, we analyse the elastic interaction between a wedge disclination dipole and a sharp crack emanating from a surface semielliptic hole by the conformal mapping technique and the complex variable method. The stress intensity factor at the tip of the crack and the image force acting on the wedge disclination dipole centre are derived. The influence of the morphology of the blunt crack and the position of the wedge disclination dipole on the shielding effect to the crack and the image force is also discussed.

2. Problem statement and solution

The current problem is shown in Fig. 1(a). A free surface $x = 0$ contains a semi-elliptic hole where its centre is located at the origin, and A and B are, respectively, the lengths of the major semi-axis and minor semi-axis of the ellipse. A sharp crack of length L–A emanates from the semi-elliptic hole along the positive x-axis. The wedge disclination dipole consists of a positive disclination with strength ω at $z_1(= x_1 + \mathrm{i}y_1 = z_0 - a\,\mathrm{e}^{\mathrm{i}\varphi})$ and a negative disclination with the same strength at $z_2(= x_2 + \mathrm{i}y_2 = z_0 + a\,\mathrm{e}^{\mathrm{i}\varphi})$ so that the dipole arm has length $2a$. Both disclination lines are perpendicular to the xoy-plane.

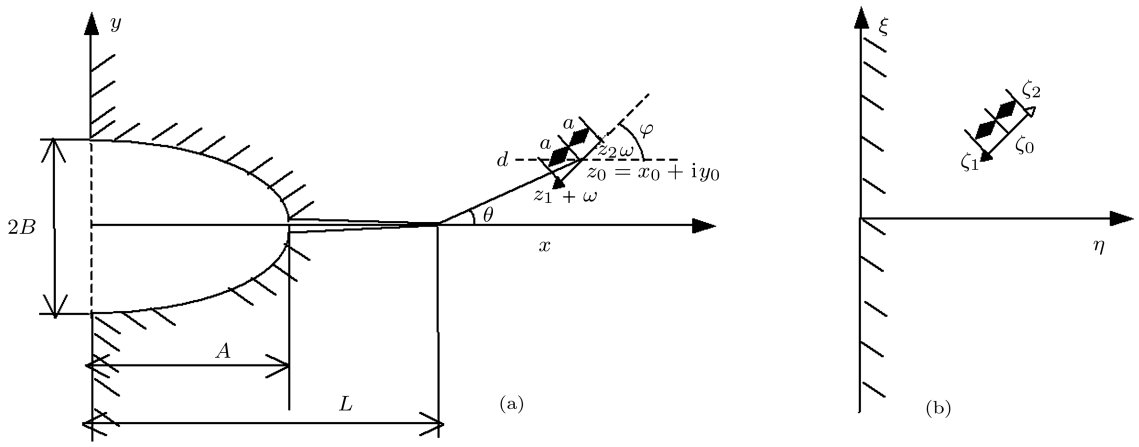


Fig. 1. An wedge disclination dipole near a sharp crack emanating from a semi-elliptic hole (a), and ζ-plane after conformal mapping (b).

For a plane strain problem, stress fields and displacement fields can be expressed in terms of two Muskhelishvili's complex potentials $\varphi(z)$ and $\psi(z)$ as follows:

$$\sigma_{xx} + \sigma_{yy} = 2[\varphi'(z) + \overline{\varphi'(z)}], \tag{1}$$

$$\sigma_{yy} - \mathrm{i}\sigma_{xy} = \varphi'(z) + \overline{\varphi'(z)} + z\overline{\varphi''(z)} + \overline{\psi'(z)}, \tag{2}$$

$$2\mu(u_x + \mathrm{i}u_y) = \kappa\varphi(z) - z\overline{\varphi'(z)} - \overline{\psi(z)}, \tag{3}$$

with $z = x + \mathrm{i}y$ and $\kappa = 3 - 4\nu$ in which μ is the shear modulus and v Poisson's ratio. The superposed bar denotes a complex conjugate, and the prime denotes differentiation with respect to argument z.

Introduce the following mapping function:[13]

$$z = \omega(\zeta) = \frac{A\sqrt{\zeta^2 + L^2} + B\sqrt{\zeta^2 + L^2 - C^4P^2}}{C^2P}, \tag{4}$$

with $\zeta = \eta + \mathrm{i}\xi, P = L/(LA - B\sqrt{L^2 - C^2})$ and $C = \sqrt{A^2 - B^2}$, which maps the surface blunt crack in the z-plane into a half space in the ζ-plane ($\eta > 0$) as shown in Fig. l(b).

With the aid of the mapping function Eq. (4), Equations (1) and (2) can be rewritten in the ζ-plane as follows:

$$\sigma_{xx} + \sigma_{yy} = 2[\Phi(\zeta) + \overline{\Phi(\zeta)}], \tag{5}$$

$$\sigma_{yy} - \mathrm{i}\sigma_{xy} = \Phi(\zeta) + \overline{\Phi(\zeta)} + \frac{\omega(\zeta)}{\overline{\omega'(\zeta)}}\overline{\Phi'(\zeta)} + \overline{\Psi(\zeta)}, \tag{6}$$

where $\Phi(\zeta) = \varphi'(\zeta)/\omega'(\zeta)$, $\Phi'(\zeta) = (\varphi''(\zeta)\omega'(\zeta) - \varphi'(\zeta)\omega''(\zeta))/[\omega'(\zeta)]^2$ and $\Psi(\zeta) = \psi'(\zeta)/\omega'(\zeta)$.

According to Ref. [5], if a wedge disclination dipole is located at an arbitrary point z_0, complex

potentials $\varphi(z)$ and $\psi(z)$ can be chosen as

$$\varphi(z) = \frac{D\omega}{2}[(z-z_1)\ln(z-z_1)-(z-z_2)\ln(z-z_2)] +\varphi_0(z), \quad (7)$$

$$\psi(z) = \frac{D\omega}{2}[\bar{z}_2\ln(z-z_2)-\bar{z}_1\ln(z-z_1)]+\psi_0(z), \quad (8)$$

where $D = \mu/2\pi(1-v)$, $\varphi_0(z)$ and $\psi_0(z)$ refer to the terms resulting from the interaction of the wedge disclination dipole with the surface blunt crack.

Substituting Eq. (4) into Eqs. (7) and (8), the complex potentials in the ζ-plane are given as

$$\varphi(\zeta) = \frac{D\omega}{2}[H_1(\zeta-\zeta_1)\ln(\zeta-\zeta_1)-H_2(\zeta-\zeta_2)\ln(\zeta-\zeta_2)] +\varphi_0(\zeta), \quad \eta>0, \quad (9)$$

$$\psi(\zeta) = \frac{D\omega}{2}[\bar{z}_2\ln(\zeta-\zeta_2)-\bar{z}_1\ln(\zeta-\zeta_1)] +\psi_0(\zeta), \quad \eta>0, \quad (10)$$

where $H_1 = \dfrac{1}{C^2P}\left(\dfrac{A\zeta_1}{\sqrt{\zeta_1^2+L^2}}+\dfrac{B\zeta_1}{\sqrt{\zeta_1^2+L^2-C^4P^2}}\right)$, and $H_2 = \dfrac{1}{C^2P}\left(\dfrac{A\zeta_2}{\sqrt{\zeta_2^2+L^2}}+\dfrac{B\zeta_2}{\sqrt{\zeta_2^2+L^2-C^4P^2}}\right)$.

Applying the Riemann–Schwarz symmetry principle, a new analytic function $\chi(\zeta)$ can be introduced as follows:

$$\chi(\zeta) = \omega(-\zeta)\frac{\varphi'(\zeta)}{\omega'(\zeta)}+\psi(\zeta), \quad \eta>0. \quad (11)$$

The substitution of Eqs. (9) and (10) into Eq. (11) yields

$$\chi(\zeta) = \frac{D\omega}{2}[-\omega(\zeta)\ln(\zeta-\zeta_1)+\omega(\zeta)\ln(\zeta-\zeta_2)] +\frac{D\omega}{2}[\bar{z}_2\ln(\zeta-\zeta_2)-\bar{z}_1\ln(\zeta-\zeta_1)]+\chi_0(\zeta). \quad (12)$$

Following Muskhelishvili's treatments, the traction-free boundary condition along the imaginary axis is satisfied by

$$\varphi(\zeta)+\frac{\omega(\zeta)}{\omega'(\zeta)}\overline{\varphi(\zeta)}+\overline{\psi(\zeta)} = 0. \quad (13)$$

To treat the boundary conditions on the interface, it is convenient to introduce the following analytic function:

$$\Omega(\zeta) = -\overline{\chi}(-\zeta) = \frac{D\omega}{2}[-\bar{\omega}(\zeta)\ln(-\zeta-\bar{\zeta}_1)+\bar{\omega}(\zeta)\ln(-\zeta-\bar{\zeta}_2)] -\frac{D\omega}{2}[z_2\ln(-\zeta-\bar{\zeta}_2)-z_1\ln(-\zeta-\bar{\zeta}_1)] +\Omega_0(\zeta), \quad \eta<0. \quad (14)$$

Using Eq. (13) together with Eq. (14), we have

$$\varphi^+(t)-\Omega^-(t) = 0, \quad (15)$$

where t denotes the point on the imaginary axis in the ζ-plane. The superscripts + and – denote the boundary values of a physical quantity when ζ approaches the imaginary axis from $\eta>0$ and $\eta<0$, respectively. Considering Eqs. (9) and (14), boundary condition Eq. (15) can be rewritten as

$$\varphi_0^+(t)-\Omega_0^-(t) = \frac{D\omega}{2}[-\bar{\omega}(\zeta)\ln(-\zeta-\bar{\zeta}_1)+\bar{\omega}(\zeta)\ln(-\zeta-\bar{\zeta}_2)]-\frac{D\omega}{2}[z_2\ln(-\zeta-\bar{\zeta}_2)-z_1\ln(-\zeta-\bar{\zeta}_1)] -\frac{D\omega}{2}[H_1(\zeta-\zeta_1)\ln(\zeta-\zeta_1)-H_2(\zeta-\zeta_2)\ln(\zeta-\zeta_2)]. \quad (16)$$

According to the Plemeij formula, we obtain

$$\varphi_0(\zeta) = \frac{D\omega}{2}[-\bar{\omega}(\zeta)\ln(-\zeta-\bar{\zeta}_1)+\bar{\omega}(\zeta)\ln(-\zeta-\bar{\zeta}_2)]-\frac{D\omega}{2}[z_2\ln(-\zeta-\bar{\zeta}_2)-z_1\ln(-\zeta-\bar{\zeta}_1)], \quad (17)$$

$$\Omega_0(\zeta) = \frac{D\omega}{2}[H_1(\zeta-\zeta_1)\ln(\zeta-\zeta_1)-H_2(\zeta-\zeta_2)\ln(\zeta-\zeta_2)]. \quad (18)$$

Substituting Eq. (17) into Eq. (9), the complex potential $\varphi(\zeta)$ is given as

$$\varphi(\zeta) = \frac{D\omega}{2}[-\bar{\omega}(\zeta)\ln(-\zeta-\bar{\zeta}_1)+\bar{\omega}(\zeta)\ln(-\zeta-\bar{\zeta}_2)]-\frac{D\omega}{2}[z_2\ln(-\zeta-\bar{\zeta}_2)-z_1\ln(-\zeta-\bar{\zeta}_1)] +\frac{D\omega}{2}[H_1(\zeta-\zeta_1)\ln(\zeta-\zeta_1)-H_2(\zeta-\zeta_2)\ln(\zeta-\zeta_2)]. \quad (19)$$

From Eqs. (14) and (18), the complex potential $\chi(\zeta)$ can be obtained to be

$$\chi(\zeta) = \frac{D\omega}{2}[-\omega(\zeta)\ln(\zeta-\zeta_1)+\omega(\zeta)\ln(\zeta-\zeta_2)] + \frac{D\omega}{2}[\bar{z}_2\ln(\zeta-\zeta_2)-\bar{z}_1\ln(\zeta-\zeta_1)]$$
$$-\frac{D\omega}{2}[\bar{H}_1(-\zeta-\bar{\zeta}_1)\ln(-\zeta-\bar{\zeta}_1)-\bar{H}_2(-\zeta-\bar{\zeta}_2)\ln(-\zeta-\bar{\zeta}_2)]. \quad (20)$$

The substitution of Eqs. (19) and (20) into Eq. (11) yields

$$\begin{aligned}
&\psi(\zeta)\\
&= \frac{A\sqrt{\zeta^2+L^2}+B\sqrt{\zeta^2+L^2-C^4P^2}}{\dfrac{A\zeta}{\sqrt{\zeta^2+L^2}}+\dfrac{B\zeta}{\sqrt{\zeta^2+L^2-C^4P^2}}}\left(\frac{D\omega}{2}\left[-\bar{\omega}'(\zeta)\ln(-\zeta-\bar{\zeta}_1)+\bar{\omega}'(\zeta)\ln(-\zeta-\bar{\zeta}_2)+\frac{\bar{\omega}(\zeta)}{-\zeta-\bar{\zeta}_1}-\frac{\bar{\omega}(\zeta)}{-\zeta-\bar{\zeta}_2}\right]\right.\\
&+\frac{D\omega}{2}\left[\frac{z_2}{-\zeta-\bar{\zeta}_2}-\frac{z_1}{-\zeta-\bar{\zeta}_1}\right]+\frac{D\omega}{2}[H_1\ln(\zeta-\zeta_1)-H_2\ln(\zeta-\zeta_2)+H_1-H_2]\Big)\\
&+\frac{D\omega}{2}[-\omega(\zeta)\ln(\zeta-\zeta_1)+\omega(\zeta)\ln(\zeta-\zeta_2)]+\frac{D\omega}{2}[\bar{z}_2\ln(\zeta-\zeta_2)-\bar{z}_1\ln(\zeta-\zeta_1)]\\
&-\frac{D\omega}{2}[\bar{H}_1(-\zeta-\bar{\zeta}_1)\ln(-\zeta-\bar{\zeta}_1)-\bar{H}_2(-\zeta-\bar{\zeta}_2)\ln(-\zeta-\bar{\zeta}_2)]. \quad (21)
\end{aligned}$$

In view of Eqs. (1)–(6) and the obtained complex potentials, the stress fields and displacement fields can be easily derived. Here we omit the details for saving space.

3. Stress intensity factors at crack tip

Stress intensity factor (SIF) near the crack tip is a very important and meaningful physical quantity. According to Zhang *et al.*[14] the stress intensity factor at the crack tip can be found from the complex stress field to be

$$K_{\rm I} - {\rm i}K_{\rm II} = 2\sqrt{2\pi}\lim_{\zeta\to 0}\sqrt{\omega(\zeta)-\omega(0)}\frac{\varphi'(\zeta)}{\omega'(\zeta)}, \quad (22)$$

with

$$\varphi'(\zeta) = \frac{D\omega}{2}\left[\bar{\omega}'(\zeta)\ln(-\zeta-\bar{\zeta}_2)-\bar{\omega}'(\zeta)\ln(-\zeta-\bar{\zeta}_1)+\frac{\bar{\omega}(\zeta)}{\zeta+\bar{\zeta}_2}-\frac{\bar{\omega}(\zeta)}{\zeta+\bar{\zeta}_1}\right]-\frac{D\omega}{2}\left(\frac{z_2}{\zeta+\bar{\zeta}_2}-\frac{z_1}{\zeta+\bar{\zeta}_1}\right)$$
$$+\frac{D\omega}{2}[H_1\ln(\zeta-\zeta_1)-H_2\ln(\zeta-\zeta_2)+H_1-H_2], \quad (23)$$

$$\omega'(\zeta) = \frac{1}{C^2P}\left(\frac{A\zeta}{\sqrt{\zeta^2+L^2}}+\frac{B\zeta}{\sqrt{\zeta^2+L^2-C^4P^2}}\right). \quad (24)$$

The substitution of Eqs. (23) and (24) into Eq. (22) yields

$$K_{\rm I} - {\rm i}K_{\rm II} = \sqrt{\pi}D\omega\frac{LCP\sqrt{L^2-C^4P^2}\sqrt{\dfrac{\dfrac{A}{L}+\dfrac{B}{\sqrt{L^2-C^4P^2}}}{P}}}{LB+A\sqrt{L^2-C^4P^2}}$$
$$\times\left(\frac{L}{\bar{\zeta}_2}-\frac{L}{\bar{\zeta}_1}+\frac{z_1}{\bar{\zeta}_1}-\frac{z_2}{\bar{\zeta}_2}+H_1\ln(-\zeta_1)-H_2\ln(-\zeta_2)+H_1-H_2\right). \quad (25)$$

Using Eq. (25), Fig. 2 shows the curves for normalised SIF $K_{\rm I0}=K_{\rm I}/10\sqrt{A}D\omega$ versus φ with different values of L/A. It is found that the wedge disclination dipole will anti-shield the tip first, and then shield it with the increase of the absolute value of φ. There exist a critical value of φ and stress intensity factor $K_{\rm I}=0$. The shielding effect is maximal around $\varphi=\pm\pi$ and the anti-shielding effect is maximal around $\varphi=0$. The shielding effect to $K_{\rm I}$ increases with the increase of L/A.

Figure 3 shows the curves for normalised SIF $K_{\rm I0}=K_{\rm I}/10\sqrt{A}D\omega$ versus θ (radian) with different

values of L/A. The anti-shielding effect increases with the increase of L/A. The anti-shielding effect is maximal around $\theta = \pm 2$.

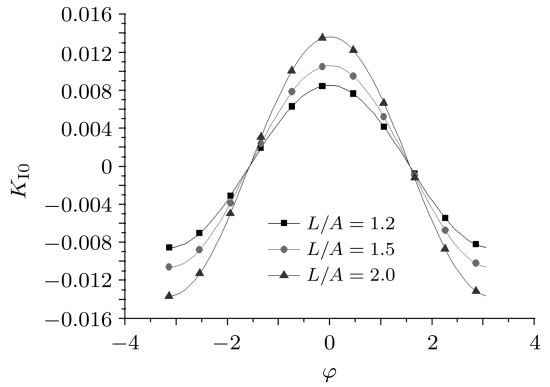


Fig. 2. Curves for normalised SIF $K_{\rm I0}$ versus θ with different values of L/A for $b_y = 0$, $A/b_x = 10^4$, $B/b_x = 10^3$, and $d/b_x = 10^3$.

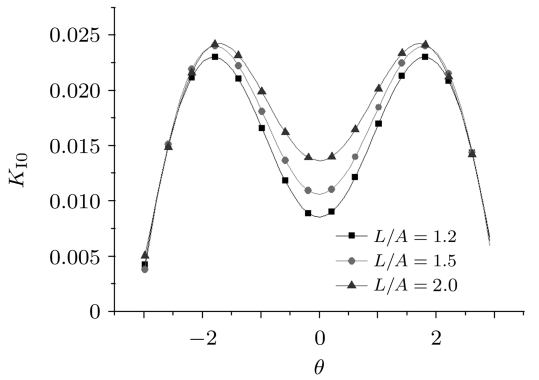


Fig. 3. Curves for normalised SIF $K_{\rm I0}$ versus θ with different values of L/A for $b_x = 0$, $A/b_y = 10^4$, $B/b_y = 10^3$, and $d/b_y = 10^3$.

The variations of the normalised SIF $K_{\rm II0} = K_{\rm II}/10\sqrt{A}D\omega$ with φ are shown in Fig. 4 with different values of B/A. It is seen that $K_{\rm II0}$ is always negative (shielding effect) when $\varphi < 0$. The shielding effect to $K_{\rm II}$ produced by the wedge disclination dipole is maximal as $\varphi = -\pi/2$ and the anti-shielding effect is maximal around at $\varphi = \pi/2$. The shielding effect to $K_{\rm II}$ also increases with the increase of B/A.

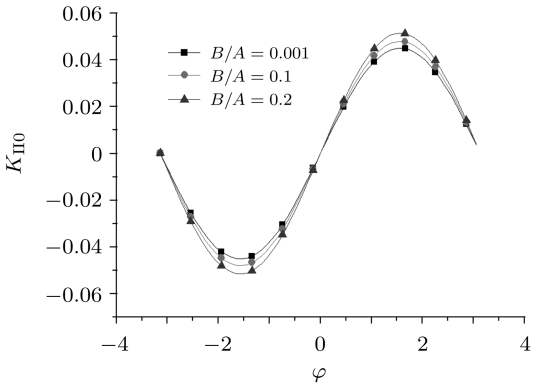


Fig. 4. Curves for normalised SIF $K_{\rm II0}$ versus θ with different values of L/A for $b_x = 0$, $A/b_y = 10^4$, $B/b_y = 10^3$, and $d/b_y = 10^3$.

4. Image force on wedge disclination dipole centre

In the present work, the force components per unit length on the disclination dipole centre can be calculated approximatively from the Peach–Koehler formula[2]

$$f_x - \mathrm{i}f_y = 2\omega a\cos\varphi\widehat{\sigma}_{xy} + 2\omega a\sin\varphi\widehat{\sigma}_{yy} + \mathrm{i}[2\omega a\cos\varphi\widehat{\sigma}_{xx} + 2\omega a\sin\varphi\widehat{\sigma}_{xy}]. \tag{26}$$

where $\widehat{\sigma}_{xx}, \widehat{\sigma}_{yy}$ and $\widehat{\sigma}_{xy}$ are the components of the perturbation stress at the disclination dipole centre in the Cartesian coordinates. The perturbation stresses can be calculated by the perturbation stress functions $\Phi_1^*(z_0)$, $\Phi_1^{*'}(z_0)$ and $\Psi_1^*(z_0)$ in the region S^+. Referring to Ref. [15] by Qaissaunee and Santare, equation (26) can be rewritten as

$$f_x - \mathrm{i}f_y = 2\omega a\,\mathrm{e}^{\mathrm{i}\varphi}[\Phi^*(\zeta_0) + \overline{\Phi^*(\zeta_0)}] + 2\omega a\,\mathrm{e}^{-\mathrm{i}\varphi}[\overline{z}_0\Phi'^*(\zeta_0) + \Psi^*(\zeta_0)]. \tag{27}$$

According to the work of Stagni, Ref. [16], the perturbation complex potentials $\Phi^*(\zeta_0)$, $\Phi'^*(\zeta_0)$ and $\Psi^*(\zeta_0)$ may be calculated as follows:

$$\Phi^*(\zeta_0) = \lim_{\zeta\to\zeta_0}\left[\frac{\varphi'(\zeta)}{\omega'(\zeta)} - \frac{\varphi_0'(\zeta)}{\omega'(\zeta)}\right], \tag{28}$$

$$\Phi^{*'}(\zeta_0) = \lim_{\zeta\to\zeta_0}\left[\frac{\varphi''(\zeta)\omega'(\zeta) - \varphi'(\zeta)\omega''(\zeta)}{[\omega'(\zeta)]^3} - \frac{\varphi_0''(\zeta)\omega'(\zeta) - \varphi_0'(\zeta)\omega''(\zeta)}{[\omega'(\zeta)]^3}\right], \tag{29}$$

$$\Psi^*(\zeta_0) = \lim_{\zeta\to\zeta_0}\left[\frac{\psi'(\zeta)}{\omega'(\zeta)} - \frac{\psi_0'(\zeta)}{\omega'(\zeta)}\right]. \tag{30}$$

The substitution of Eqs. (23) and (24) into Eqs. (28)–(30) yields

$$\Phi^*(\zeta_0) = \frac{\dfrac{D\omega}{2}\left[\bar{\omega}'(\zeta)\ln(-\zeta-\bar{\zeta}_2)-\bar{\omega}'(\zeta)\ln(-\zeta-\bar{\zeta}_1)+\dfrac{\bar{\omega}(\zeta)}{\zeta+\bar{\zeta}_2}-\dfrac{\bar{\omega}(\zeta)}{\zeta+\bar{\zeta}_1}\right]-\dfrac{D\omega}{2}\left(\dfrac{z_2}{\zeta+\bar{\zeta}_2}-\dfrac{z_1}{\zeta+\bar{\zeta}_1}\right)}{\dfrac{1}{C^2P}\left(\dfrac{A\zeta_0}{\sqrt{\zeta_0^2+L^2}}+\dfrac{B\zeta_0}{\sqrt{\zeta_0^2+L^2-C^4P^2}}\right)}, \tag{31}$$

$$\begin{aligned}\Phi^{*'}(\zeta_0) = {} & \frac{D\omega}{2\left[\dfrac{1}{C^2P}\left(\dfrac{A\zeta_0}{\sqrt{\zeta_0^2+L^2}}+\dfrac{B\zeta_0}{\sqrt{\zeta_0^2+L^2-C^4P^2}}\right)\right]^2}\left[\frac{\bar{\omega}'(\zeta)(\zeta+\bar{\zeta}_1)-\bar{\omega}(\zeta)}{(\zeta+\bar{\zeta}_1)^2}-\frac{\bar{\omega}'(\zeta)(\zeta+\bar{\zeta}_2)-\bar{\omega}(\zeta)}{(\zeta+\bar{\zeta}_2)^2}\right.\\ & \left.+\bar{\omega}''(\zeta)\ln(-\zeta-\bar{\zeta}_2)-\bar{\omega}''(\zeta)\ln(-\zeta-\bar{\zeta}_1)+\frac{\bar{\omega}'(\zeta)}{\zeta+\bar{\zeta}_2}-\frac{\bar{\omega}'(\zeta)}{\zeta+\bar{\zeta}_1}+\frac{z_2}{(\zeta+\bar{\zeta}_2)^2}-\frac{z_1}{(\zeta+\bar{\zeta}_1)^2}\right]\\ & -\frac{\left(\dfrac{A(\zeta_0^2+L^2)-A\zeta_0^2}{(\zeta_0^2+L^2)^{3/2}}+\dfrac{B(\zeta_0^2+L^2-C^4P^2)-B\zeta_0^2}{(\zeta_0^2+L^2-C^4P^2)^{3/2}}\right)}{\dfrac{1}{C^4P^2}\left[\left(\dfrac{A\zeta_0}{\sqrt{\zeta_0^2+L^2}}+\dfrac{B\zeta_0}{\sqrt{\zeta_0^2+L^2-C^4P^2}}\right)\right]^3}\frac{D\omega}{2}\left[\frac{\bar{\omega}(\zeta)}{\zeta+\bar{\zeta}_2}-\frac{\bar{\omega}(\zeta)}{\zeta+\bar{\zeta}_1}+\bar{\omega}'(\zeta)\ln(-\zeta-\bar{\zeta}_2)\right.\\ & \left.-\bar{\omega}'(\zeta)\ln(-\zeta-\bar{\zeta}_1)-\frac{z_2}{\zeta+\bar{\zeta}_2}+\frac{z_1}{\zeta+\bar{\zeta}_1}\right],\end{aligned} \tag{32}$$

$$\begin{aligned}\Psi^*(\zeta_0) = {} & \frac{A\sqrt{\zeta_0^2+L^2}+B\sqrt{\zeta_0^2+L^2-C^4P^2}}{\dfrac{1}{C^2P}\left(\dfrac{A\zeta_0}{\sqrt{\zeta_0^2+L^2}}+\dfrac{B\zeta_0}{\sqrt{\zeta_0^2+L^2-C^4P^2}}\right)^2}\frac{D\omega}{2}\left[\frac{\bar{\omega}'(\zeta)(\zeta+\bar{\zeta}_1)-\bar{\omega}(\zeta)}{(\zeta+\bar{\zeta}_1)^2}-\frac{\bar{\omega}'(\zeta)(\zeta+\bar{\zeta}_2)-\bar{\omega}(\zeta)}{(\zeta+\bar{\zeta}_2)^2}\right.\\ & \left.+\bar{\omega}''(\zeta)\ln(-\zeta-\bar{\zeta}_2)-\bar{\omega}''(\zeta)\ln(-\zeta-\bar{\zeta}_1)+\frac{\bar{\omega}'(\zeta)}{\zeta+\bar{\zeta}_2}-\frac{\bar{\omega}'(\zeta)}{\zeta+\bar{\zeta}_1}+\frac{z_2}{(\zeta+\bar{\zeta}_2)^2}-\frac{z_1}{(\zeta+\bar{\zeta}_1)^2}\right]\\ & +\left[\frac{C^2P\left(\dfrac{A(\zeta_0^2+L^2)-A\zeta_0^2}{(\zeta_0^2+L^2)^{3/2}}+\dfrac{B(\zeta_0^2+L^2-C^4P^2)-B\zeta_0^2}{(\zeta_0^2+L^2-C^4P^2)^{3/2}}\right)\left(A\sqrt{\zeta_0^2+L^2}+B\sqrt{\zeta_0^2+L^2-C^4P^2}\right)}{\left[\left(\dfrac{A\zeta_0}{\sqrt{\zeta_0^2+L^2}}+\dfrac{B\zeta_0}{\sqrt{\zeta_0^2+L^2-C^4P^2}}\right)\right]^3}\right.\\ & \left.-\frac{C^2P}{\left(\dfrac{A\zeta_0}{\sqrt{\zeta_0^2+L^2}}+\dfrac{B\zeta_0}{\sqrt{\zeta_0^2+L^2-C^4P^2}}\right)}\right]\frac{D\omega}{2}\left[-\bar{\omega}'(\zeta)\ln(-\zeta-\bar{\zeta}_1)+\bar{\omega}'(\zeta)\ln(-\zeta-\bar{\zeta}_2)\right.\\ & \left.+\frac{\bar{\omega}(\zeta)}{-\zeta-\bar{\zeta}_1}-\frac{\bar{\omega}(\zeta)}{-\zeta-\bar{\zeta}_2}+H_1-H_2+\frac{z_2}{-\zeta-\bar{\zeta}_2}-\frac{z_1}{-\zeta-\bar{\zeta}_1}\right]\\ & -\frac{\dfrac{D\omega}{2}[-\bar{H}_1\ln(-\zeta-\bar{\zeta}_1)+\bar{H}_2\ln(-\zeta-\bar{\zeta}_2)-\bar{H}_1+\bar{H}_2]}{\dfrac{1}{C^2P}\left(\dfrac{A\zeta_0}{\sqrt{\zeta_0^2+L^2}}+\dfrac{B\zeta_0}{\sqrt{\zeta_0^2+L^2-C^4P^2}}\right)}.\end{aligned} \tag{33}$$

Now the detailed expression of the image force can be found from Eq. (27) together with Eqs. (31)–(33).

In the following discussion, we consider the case where the wedge disclination dipole lies on the x-axis ($z_0 = x_0 > L$). Figure 5 shows the curves for normalised image force $f_{x0} = f_x/D\omega^2 a$ versus x_0/L with different values of L/A. It can be found that the normalised image force f_{x0} is always negative, which means that the wedge disclination dipole is always attracted by the crack. The attraction force acting on the wedge disclination dipole decreases with L/A and x_0/L increasing. Figure 6 shows the variations of normalised image force $f_{x0} = f_x/D\omega^2 a$ with B/A for different values of L/A and z_0/L. It is seen from Fig. 6 that the attraction force acting on the wedge disclination dipole increases with the increase of B/A, while the attraction force decreases with L/A and x_0/L increasing.

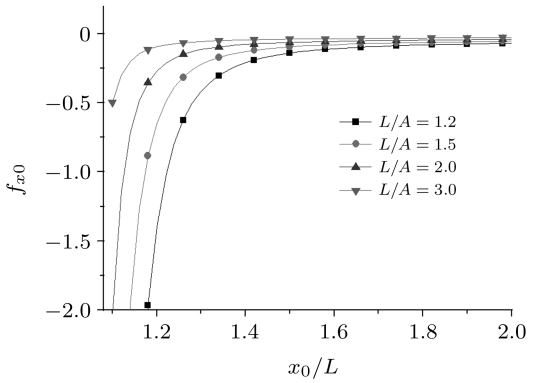


Fig. 5. Variations of normalised image force f_{x0} with x_0/L for different values of L/A at $A = 1$, $B = 0.1$, and $b_y = 0$.

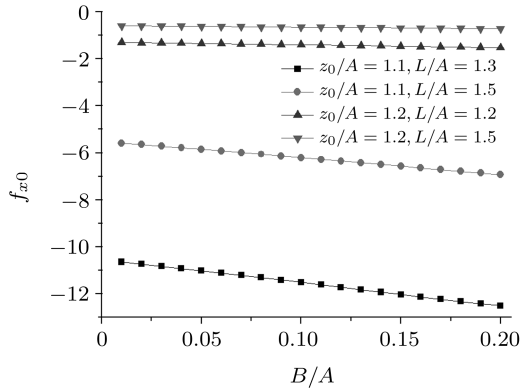


Fig. 6. Variations of normalised image force f_{x0} with B/A for different values of L/A and z_0/L at $A = 1$, and $b_y = 0$.

5. Conclusions

The problem of a wedge disclination dipole interacting with a sharp crack emanating from a surface semielliptic hole is solved by the conformal mapping technique and the complex variable method. The closed form solutions are derived for complex potentials and stress fields. The stress intensity factor at the tip of the crack and the image force acting on the wedge disclination dipole centre are also calculated. The influence of the morphology of the blunt crack and the position of the wedge disclination dipole on the shielding effect to the crack and the image force is discussed.

The results show that the wedge disclination dipole can reduce SIF $K_{\rm I}$ at the tip of the crack (shielding effect) only when $|\varphi| > \pi/2$ and the wedge disclination dipole can reduce SIF $K_{\rm II}$ at the tip of the crack only when $\varphi > 0$. The shielding or anti-shielding effect to the stress intensity factor increases when the wedge disclination dipole approaches the tip of the crack. In addition, the effect of the morphology of the crack on the image force on the wedge disclination dipole center is very significant. The attraction force produced by the blunt crack increases with the increase of B/A but decreases with L/A and x_0/L increasing.

References

[1] Romanov A E 1993 *Materials Science & Engineering* A **164** 58
[2] Zhu T, Li J and Yip S 2004 *Phys. Rev. Lett.* **93** 025503
[3] Gilra N K 1977 *Crystal Lattice Defects* **7** 23
[4] Song H P, Fang Q H and Liu Y W 2008 *Chin. Phys.* B **17** 4592
[5] Fang Q H and Liu Y W 2006 *Phys. Status Solidi.* A **203** 443
[6] Weertman J 1996 *Dislocation Based Fracture Mechanics* (Singapore: World Scientific)
[7] Song H P, Fang Q H and Liu Y W 2009 *Chin. Phys.* B **18** 1564
[8] Chen B T, Zhang T Y and Lee S 1999 *Mech. Mater.* **31** 71
[9] Song H P, Fang Q H and Liu Y W 2009 *Eng. Fract. Mech.* **76** 1603
[10] Vehoff H and Neumann P 1979 *Acta Metall.* **27** 915
[11] Ohr S M 1985 *Mater. Sci. Eng.* **72** 1
[12] Shiue S T and Lee S 1989 *Phys. Status Solidi* A **113** 365
[13] Yang Y S, Lee S L and Lan B T 1995 *Eng. Fract. Mech.* **52** 83
[14] Zhang T Y, Tong P, Hao O and Lee S 1995 *J. Appl. Phys.* **78** 4873
[15] Qaissaunee M T and Santare M H 1995 *Quarter J. Mech. Appl. Math.* **48** 465
[16] Stagni L 1993 *Philos. Mag.* A **68** 49